Nanoparticulate coatings for enhanced cyclability of LiCoO$_2$ cathodes

George Ting-Kuo Fey [a,*], Cheng-Zhang Lu [a], Jiun-Da Huang [a],
T. Prem Kumar [a,1], Yu-Chen Chang [b]

[a] *Department of Chemical and Materials Engineering, National Central University, Chung-Li 32054, Taiwan, ROC*
[b] *Department of Chemical Engineering, Yuan-Ze University, Taoyuan, Nelli 301, Taiwan, ROC*

Abstract

Surface modification as a method for enhancing the cyclability of LiCoO$_2$ cathodes is reviewed. The performances of TiO$_2$ and ZrO$_2$, and their mixed oxide, ZrTiO$_4$, as coating materials, are compared. Coating techniques such as sol–gel and mechano-thermal processes are described. Structural data and morphology of the oxide-coated LiCoO$_2$ are correlated with electrochemical behavior. Their enhanced cyclability is attributed to the suppression of the cycle-limiting phase transitions accompanying the charge–discharge processes. The higher cyclability of the mixed oxide-coated cathodes over those coated with the corresponding individual oxides is also demonstrated. It is also shown that the nature of the core material and the sol–gel precursors for the coatings play a definitive role in the electrochemical behavior of the coated cathode materials.

1. Introduction

Battery research today focuses on the synthesis of novel active materials, as well as improvements in currently available materials. Layered LiCoO$_2$, the most popular cathode material in lithium batteries, can cycle only 0.5 Li per host molecule. However, delithiation of LiCoO$_2$ increases the electrostatic repulsion between adjacent oxygen layers in the host lattice [1,2]. The accompanying anisotropic volume change causes a structural degradation of the host material [3], leading to large capacity fades upon repeated cycling [4,5].

Several groups have demonstrated the enhanced cyclability of LiCoO$_2$ coated with a thin layer of an oxide such as Al$_2$O$_3$ [6–10], B$_2$O$_3$ [8], MgO [11–13], SnO$_2$ [14], TiO$_2$ [8,10] and ZrO$_2$ [8,10]. The improved structural stability of the core material is attributed to substitutional oxides on the cathode surface [12,14], as well as

to the suppression of cycle-limiting phase transitions associated with the intercalation–deintercalation processes by high fracture-tough coating materials [8]. Moreover, the presence of an inert oxide coating on the cathode particle can prevent direct contact of the active material with the electrolyte, limiting the dissolution of cobalt in the electrolyte [11,15]. The general coating procedures adopted in the above studies are based on an in situ sol–gel or precipitation technique. Recently, we demonstrated a simple and economical mechano-thermal process by which pre-formed nanoparticles are deposited on commercial LiCoO$_2$ powders [16–18].

In this paper, we compare performance of LiCoO$_2$ coated by sol–gel and mechano-thermal processes. TiO$_2$ and ZrO$_2$ were selected as the representative coating materials. The effect of ZrTiO$_4$ coating is compared with the individual oxide coatings. The effect of Al$_2$O$_3$ derived from various precursors as a coating material is also presented.

2. Experimental

LiCoO$_2$ powder, with an average particle of size 1–8 μm, was a commercial product of Coremax Taiwan Corporation.

* Corresponding author. Tel.: +886 3 425 7325/+886 3 422 7151x34206; fax: +886 3 425 7325.
    E-mail address: gfey@cc.ncu.edu.tw (G.T.-K. Fey).
[1] Present address: Central Electrochemical Research Institute, Karaikudi 630006, Tamil Nadu, India.

A polymeric sol–gel method [19] was adopted for the coating with TiO_2, ZrO_2 and $ZrTiO_4$, as described in our earlier papers [20–22]. For the mechano-thermal coating process, pre-formed nanoparticles of the respective oxides were used. The TiO_2 samples were P25 samples from Degussa AG (particle size: 21 nm), as well as TiO_2 samples of various particle sizes prepared by chemical vapor deposition (from Yuan-Ze University). ZrO_2 samples were from the Nanotechnology Laboratory, National Central University (particle size: 30 nm) and two samples from the spray pyrolysis facility at the Yuan-Ze University (500 and 600 nm). The mechano-thermal coating procedure has been described elsewhere [16–18]. The ratios of $LiCoO_2$ to the coated oxide employed were 99.9:0.1, 99.7:0.3, 99.0:1.0 and 98.0:2.0.

An X-ray diffractometer (Siemens D-5000, Mac Science MXP18) was used for structural analysis. BET surface area measurements were carried out on a Micromeritics ASAP 2010 surface area analyzer. The microstructures of the coated particles were examined by a JEOL JEM-4000EX high-resolution transmission electron microscope. Depth profiles of titanium, zirconium, cobalt and oxygen in the coated materials were recorded by ESCA (VG Scientific ESCALAB 250).

Galvanostatic charge–discharge of the cathode materials were studied in 2032-type coin cells at 0.1 or $0.2C$ (with respect to a theoretical capacity of $274 \, \text{mAh g}^{-1}$) between 2.75 and 4.40 V in a multi-channel battery tester (Maccor 4000). Phase transitions occurring during the cycling processes were examined by slow scan cyclic voltammetry on a Solartron 1287 Electrochemical Interface at a scan rate of $0.1 \, \text{mV s}^{-1}$ between 3.0 and 4.4 V. Details of cell construction are given elsewhere [16–18].

3. Results and discussion

3.1. X-ray diffraction

The diffraction patterns of all the coated particles conformed to the $\overline{R3}m$ symmetry of the core material, irrespective of the coating material, coating level or the coating method, because the coating material was present as a thin film, possibly as a mixed oxide formed by interaction of the coating oxide with the core $LiCoO_2$. This, together with the larger values of the c parameter for the coated samples (Table 1), suggests the formation of solid solutions incorporating ions with larger crystal ionic radii (Zr^{4+}: 0.86 Å; Ti^{4+}: 0.745 Å and Co^{3+}: 0.685 Å). Cho et al. [14] speculate that nominally pure $LiCoO_2$ is defective and contains a small fraction of Co^{4+}, which could be compensated for by vacancies in the cobalt sublattice. According to these authors [14], the substitution of a tetravalent ion is possible in the interstitial Co^{4+} sites. Thus, we expect that an inter-oxide film of composition $LiM_yCo_{1-y}O_{2+0.5y}$ (M = Ti or Zr) to form on the surface.

Table 1
Crystallographic data and R-factor values for bare and coated $LiCoO_2$

Coating	a (Å)	c (Å)	c/a	R-factor
$y = 0.0$	2.810	13.938	4.96	0.77
Sol–gel method				
ZrO_2; $y = 1.0$	2.812	13.972	4.99	0.46
TiO_2; $y = 1.0$	2.821	13.862	4.91	0.49
$ZrTiO_4$; $y = 1.0$	2.834	13.841	4.88	0.46
Sol–gel method				
ZrO_2; $y = 0.1$	2.811	13.974	4.97	0.50
ZrO_2; $y = 0.3$	2.814	14.001	4.98	0.45
ZrO_2; $y = 1.0$	2.812	13.972	4.99	0.46
ZrO_2; $y = 2.0$	2.806	13.913	4.96	0.66
Mechano-thermal method				
ZrO_2; $y = 0.1$	2.824	14.013	4.96	0.73
ZrO_2; $y = 0.3$	2.827	14.029	4.96	0.67
ZrO_2; $y = 1.0$	2.834	14.104	4.98	0.58
ZrO_2; $y = 2.0$	2.825	14.044	4.97	0.77

$(1 - y)$ wt.% $LiCoO_2 + y$ wt.% coating material.

Dahn et al. [23,24] suggested that the R-factor, defined as the ratio of the intensities of the hexagonal characteristic doublet peaks $(0\,0\,6)$ and $(1\,0\,2)$ to the $(1\,0\,1)$ peak, is an indicator of hexagonal ordering. The values of the R-factor for all the coated samples were invariably lower than the R-factor of the bare $LiCoO_2$ (Table 1). However, it must be mentioned that except for the ZrO_2-coated $LiCoO_2$ (sol–gel), all the other materials had the lowest R-factor values at 1.0 wt.% coating level. The lowest R-factor value for the ZrO_2-coated $LiCoO_2$ (sol–gel) was at 0.3 wt.%.

3.2. Microstructure and surface area

Fig. 1 is an HRTEM image of a 1.0 wt.% TiO_2-coated $LiCoO_2$ particle coated by the mechano-thermal process. The coating material formed a compact kernel of 60 nm thickness around the $LiCoO_2$ particle. Similar compact coatings were observed with other coated particles.

The BET surface area of the bare $LiCoO_2$ was $0.62 \, \text{m}^2 \, \text{g}^{-1}$ and that of a 1.0 wt.% TiO_2-coated $LiCoO_2$ (mechano-thermal) was $1.26 \, \text{m}^2 \, \text{g}^{-1}$. Considering that the surface area of the TiO_2 nanoparticles was $50 \pm 15 \, \text{m}^2 \, \text{g}^{-1}$, an increase in the surface area of the coated particles by $0.64 \, \text{m}^2 \, \text{g}^{-1}$ is commensurate with $0.50 \pm 0.15 \, \text{m}^2 \, \text{g}^{-1}$ that may be expected from a 1.0 wt.% coating of TiO_2 particles.

3.3. ESCA depth profiles

The spatial distributions of the constituent ions in the coated particles were examined by an ESCA depth profile analysis. The results of the analysis on TiO_2-coated (1.0 wt.%, mechano-thermal) $LiCoO_2$ particles are displayed in Fig. 2. The concentration of Ti was low, its depth profile highlighted in the inset. The concentration of Co increased up to a certain depth and then leveled off. It can be seen that the concentration of Ti dropped from the surface to nearly
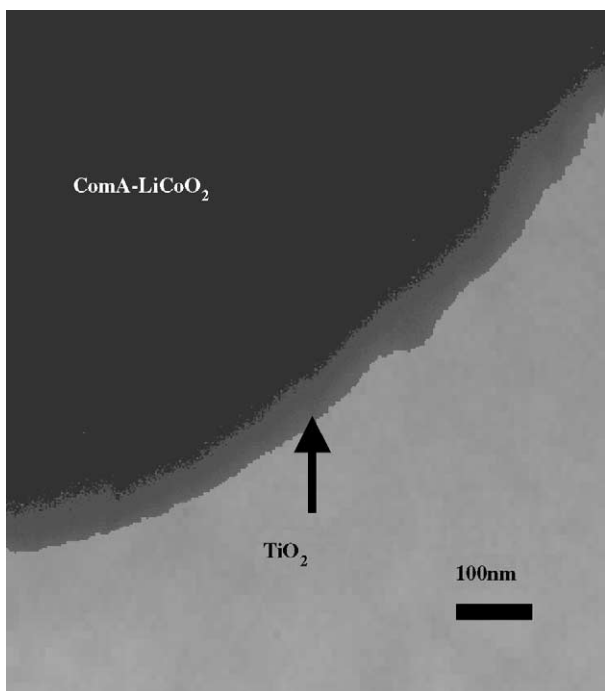
Fig. 1. An HRTEM image of a 1.0 wt.% TiO_2-coated $LiCoO_2$ particle (mechano-thermal method).

zero, at a depth actually corresponding to the thickness of the coatings as seen from the HRTEM study. The depth profiles suggest that the cations in the coating material diffused into the bulk of the cathode-active particle during calcination. This supposition is attested to by our XRD results, which suggest the formation of substitutional surface oxides. Similar results were obtained with $LiCoO_2$ coated with ZrO_2 and $ZrTiO_4$.
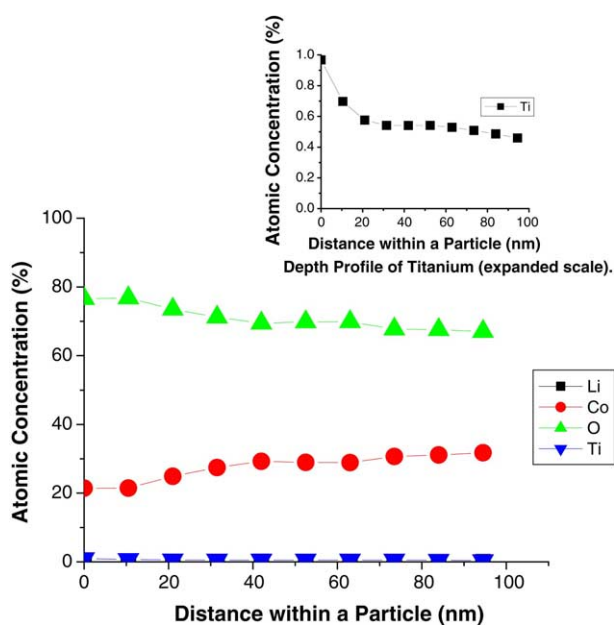

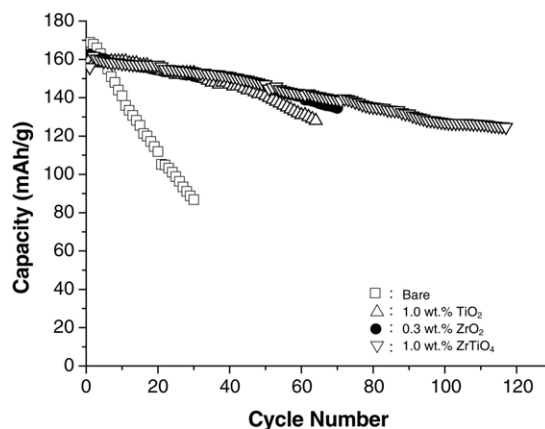Fig. 2. ESCA depth profiles of $LiCoO_2$ coated with TiO_2.

Fig. 3. Cycling behavior of bare and sol–gel coated $LiCoO_2$.

3.4. Galvanostatic charge–discharge studies

3.4.1. Sol–gel coatings

Cycling data on the coated materials show that the optimal coating level was the one at which the R-factor was the lowest, suggesting that a good hexagonal ordering of the host lattice favored the reversible intercalation of lithium. For example, the data on the $ZrTiO_4$-coated $LiCoO_2$ (sol–gel method) showed that the cyclability was commensurate with the R-factor value. The R-factor values and cyclability (for a cut-off value of 80% for the capacity retention) for the $ZrTiO_4$-coated materials were as follows: coating level 0.0 wt.%: 0.51, 12 cycles; coating level 0.1 wt.%: 0.49, 62 cycles; coating level 1.0 wt.%: 0.46, 117 cycles and coating level 3.0 wt.%: 0.50, 43 cycles. For all the coated materials, the cyclability increased with a decrease in the R-factor value.

Fig. 3 shows the cycling behavior of $LiCoO_2$ coated with ZrO_2, TiO_2 and $ZrTiO_4$. The coating levels were 1.0 wt.% for TiO_2 and $ZrTiO_4$ and 0.3 wt.% for ZrO_2, the coating levels at which the R-factor values were the lowest. The first-cycle capacities of the coated samples were 162, 160 and 156 mAh g^{-1} for coatings of ZrO_2, TiO_2 and $ZrTiO_4$, respectively. The cyclabilities of the respective materials (for an 80% cut-off value based on their first-cycle capacities) were 93, 64 and 117 cycles. These represent 8-, 5- and 10-fold improvement in the cyclability, compared to the bare $LiCoO_2$ (12 cycles; first-cycle capacity: 169 mAh $^{-1}$g). It must be noted that the reduced first-cycle capacities of the coated materials were due to the reduced number of active Co^{3+} ions in the cathode material, as well as to a slight decrease in the capacity utilization because of the insulating surface layer on the particles. The superior performance of the mixed oxide, $ZrTiO_4$, can be noted.

3.4.2. Mechano-thermal coatings

Fig. 4 shows the charge–discharge behavior of $LiCoO_2$ mechano-thermally coated with nanoparticulate ZrO_2, TiO_2 and $ZrTiO_4$. The coating level was fixed at 1.0 wt.%, that was the level at which the R-factor values were the lowest.
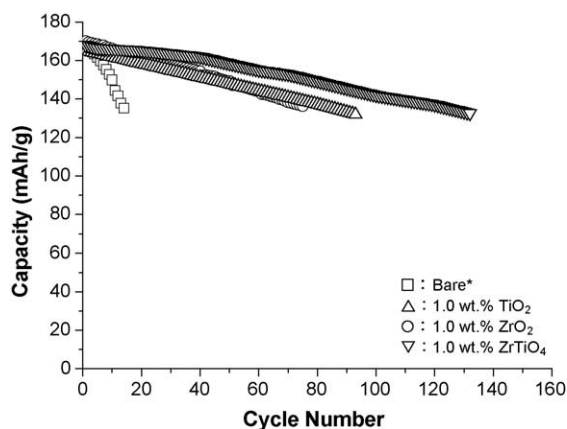
Fig. 4. Cycling behavior of bare and mechano-thermally coated LiCoO$_2$.

Fig. 5. Cycling behavior of LiCoO$_2$ coated by the sol–gel and mechano-thermal methods. Coating level: 1.0 wt.%.

Table 2
Cycling data on LiCoO$_2$ coated with ZrO$_2$ of different particle sizes

Particle size (nm)	First-cycle capacity (mAh g^{-1})	Number of cycles for 80% cut-off in capacity
30	164	110
500	166	24
600	172	37

Coating level: 1.0 wt.%.

The particle sizes of the ZrO$_2$, TiO$_2$ and ZrTiO$_4$ prepared by the sol–gel method were 50, 40 and 30 nm, respectively. The first-cycle capacities of the coated materials were slightly lower than the first-cycle capacity of bare LiCoO$_2$ (ZrO$_2$-coated: 167 mAh g^{-1}; TiO$_2$-coated: 165 mAh g^{-1} and ZrTiO$_4$-coated: 168 mAh g^{-1}). However, the higher cyclability of the mixed oxide-coated cathodes over those coated with the corresponding individual oxides was obtained by employing either the sol–gel or mechano-thermal coating method. For instance, while the cyclability improved to 75 and 93 cycles with the materials coated with ZrO$_2$ and TiO$_2$, respectively (a six- and eight-fold improvement), the improvement in cyclability with the ZrTiO$_4$-coated material was 10-fold (128 cycles), thus demonstrating the superiority of the mixed oxide as a coating material over the individual ones.

3.4.3. Effect of particle size

Tables 2 and 3 illustrate the effect of particle size on cycling behavior of mechano-thermally coated LiCoO$_2$. It was found that the optimal coating level with the 30 nm ZrO$_2$ par-

ticles was 1.0 wt.%, while that for the large spray-pyrolyzed ZrO$_2$ particles (500 and 600 nm) was 0.3 wt.%. Obviously, the nanoparticulate ZrO$_2$ formed a more uniform and compact film than the large ZrO$_2$ particles did. The importance of nanoparticles as coatings is demonstrated by this behavior.

Table 3 gives data on the particle size and crystallographic form on the nanoparticulate TiO$_2$ coating materials, as well as cycling data on LiCoO$_2$ coated with these nanoparticles (coating level: 1.0 wt.%). It appears that not only the particle size but also the allotropic modification of the material affects the coating behavior. In fact, the rutile, anatase and brookite forms of TiO$_2$ have different electrochemical characteristics [25,26]. A study of the table suggests the superiority of anatase over rutile in enhancing the cyclability of LiCoO$_2$.

3.4.4. Effect of coating method

Fig. 5 illustrates the effect of the coating method on the cyclability of the coated cathodes. It is clearly seen that the individual and mixed oxides performed better as a coating material when they were applied by the mechano-thermal method. In the case of ZrO$_2$, the number of cycles for an 80% cut-off was 75 for the mechano-thermally coated material, which is higher than the 70 cycles that the sol–gel coated material could deliver. Similarly, in the case of TiO$_2$, improved cyclability was noted with the mechano-thermal coating method (93 cycles) compared to the sol–gel method (64 cycles). Furthermore, the cyclability with the ZrTiO$_4$-coated cathodes

Table 3
Particle size and phase composition of TiO$_2$ particles and cycling behavior of LiCoO$_2$ coated with them

Sample	Particle size (nm)	Composition (%)		Cycling behavior	
		Anatase	Rutile	First-cycle capacity (mAh g^{-1})	Cyclability* (cycles)
CVD-A	21.7	Trace	99.9	168	84
CVD-B	35.0	31.3	68.7	165	89
CVD-C	21.5	8.3	91.7	162	70
CVD-D	5.0–20.0	65.1	34.9	166	60
Degussa P25	21.0	75.0	25.0	156	144

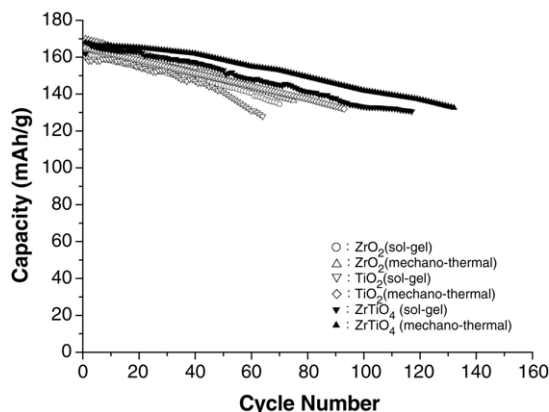* The number of cycles the material sustains before it reaches 80% of its initial capacity.

Table 4
Cycling behavior of LiCoO₂ samples coated with Al₂O₃ derived from various precursors

Core material	Al₂O₃ precursor	Cycling rate	First-cycle capacity (mAh g⁻¹)	Cyclability (80% C.R.)
LiCoO₂-I	Uncoated LiCoO₂	$0.1C$	167	26
LiCoO₂-I	Al-polyoxohydroxy cations	$0.1C$	168	257
LiCoO₂-II	Uncoated LiCoO₂	$0.1C$	171	14
LiCoO₂-II	Al-*tert*-butoxide	$0.1C$	165	28
LiCoO₂-II	Uncoated LiCoO₂	$0.2C$	169	12
LiCoO₂-II	Carboxylate alumoxane	$0.2C$	159	185

Coating method: sol–gel. LiCoO₂-I: commercial sample purchased from FMC. LiCoO₂-II: commercial sample purchased from Comax.

using the mechano-thermally coating method (132 cycles) was higher than that using the sol–gel coating method (117 cycles). These results suggest that the mechano-thermal coating process produces materials with better electrochemical characteristics. Moreover, the mechano-thermal coating process is a simple, inexpensive and commercially viable one. These advantages must be viewed against a backdrop of demerits of the sol–gel process, which includes the use of expensive alkoxide precursors like *sec*-butoxides and ethylhexanate diisopropoxides, generation of the green bodies in organic solvents like *iso*-propanol, and the release of environmentally hazardous solvent and alcoholic by-products during the evaporation and calcination processes. Thus, the mechano-thermal coating process can be an economic, convenient and clean alternative to the sol–gel coating process.

3.4.5. Effect of substrate and sol–gel coating precursor

Table 4 is a summary of our results with two commercial LiCoO₂ samples (designated I and II, respectively, for FMC and Comax) sol–gel coated with Al₂O₃ derived from a variety of precursors. It is clear that the nature of both the core material and the coatings (obtained from different precursors) have a definite effect on the electrochemical behavior of the coated LiCoO₂ materials. It is seen from Table 4 that the best performance—in terms of the number of cycles at $0.2C$ rate—was obtained with LiCoO₂ coated with alumina derived from carboxylate alumoxanes [27]. It is pertinent to note here that carboxylate alumoxanes are formed by reaction of boehmite with carboxylic acids in which nanoparticulate fragments of boehmite are stabilized by replacing its oxide and hydroxide groups with carboxylate groups [28,29]. Thermolysis of carboxylate alumoxanes yields alumina [29,30]. Effectively, we are coating LiCoO₂ with nanoparticulate carboxylate alumoxanes in sol form prior to decomposing the coating into one of alumina. Specifically, the precursor used in this example was derived by the reaction of boehmite with (methoxyethoxy)acetic acid [27].

3.5. Cyclic voltammetry

The fade in capacity with cycling of LiCoO₂ cathodes is attributed to a hexagonal–monoclinic–hexagonal phase transition above 4.1 V versus Li⁺/Li [3–5]. Fig. 6a presents the cyclic voltammograms of the bare LiCoO₂, while that of

a 1.0 wt.% ZrTiO₄-coated LiCoO₂ sample (sol–gel) is presented in Fig. 6b. While the peaks corresponding to the phase transitions persist in every cycle for the bare LiCoO₂, such peaks can be observed only in the first cycle for the coated LiCoO₂. In the case of all the coated materials, the peaks were seen distinctly suppressed from the second cycle onwards.

The suppression of the peaks with cycling indicates that any defect in the coating that might have been present initially got repaired upon repeated cycling. The presence of cracks, pinholes and other coating defects on coated surfaces
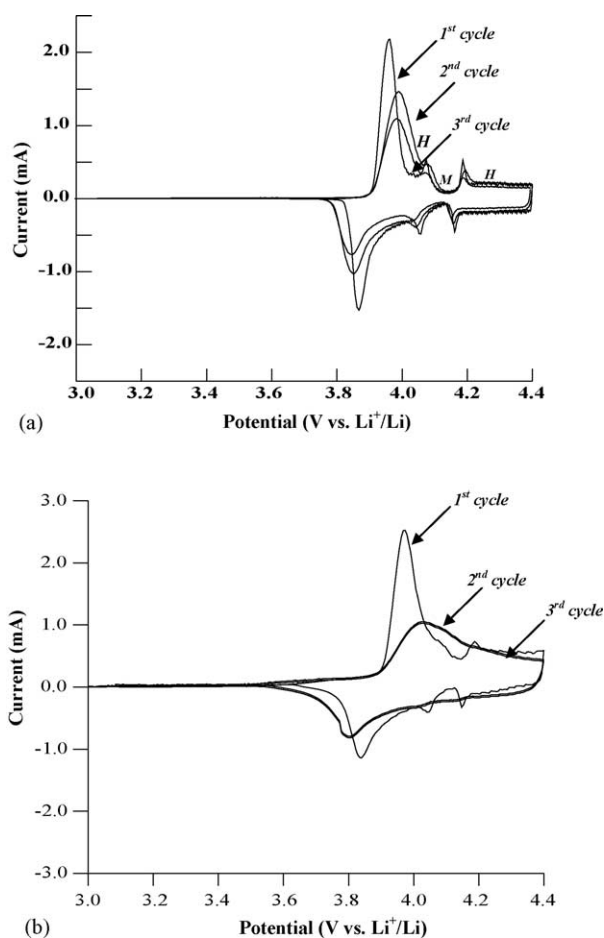

Fig. 6. Slow scan cyclic voltammograms of (a) bare LiCoO₂ and (b) 1.0 wt.% ZrTiO₄-coated LiCoO₂. Coating method: sol–gel.

is inevitable, but such defects may form and close with the application of a load, or upon thermal cycling. Thus, as the lattice contracts and expands during the cycling processes, the surface texture of the active material particles changes, enabling the coating material to become ingrained in the crevices and cracks on the cathode surface. The more compact kernel that results leads to a suppression of the phase transitions, enhancing the cyclability of the coated material. The absence of phase transitions in the coated samples ensures negligible strain, resulting in a longer cycle life.

4. Conclusions

A commercial $LiCoO_2$ sample was coated with ZrO_2, TiO_2 and $ZrTiO_4$ by sol–gel and mechano-thermal procedures. XRD data of the coated samples suggested the formation of substitutional compounds of the composition $Li_xM_yCo_{1-y}O_{2+0.5y}$ (M = Ti and/or Zr) on the surface of the cathode. Electron microscopic images of the coated particles revealed that the oxide formed a compact coating over the cathode particles. Galvanostatic charge–discharge studies suggested that the maximum cyclability was realized with the coated materials that had the lowest R-factor values. In general, the mechano-thermal method yielded products with greater cyclability than those obtained by the sol–gel method. Typically, the sol–gel method yielded about a five-fold improvement with TiO_2 and ZrO_2 while the corresponding improvements with the mechano-thermal coating method were eight- and six-fold. In the case of the $ZrTiO_4$ coatings, the improvement in cycling with the sol–gel and mechano-thermal methods were 8- and 10-fold, respectively. Cyclic voltammetric studies showed that the coating led to a suppression of the cycle-limiting phase transitions accompanying the charge–discharge processes. Studies with the mixed oxide, $ZrTiO_4$, showed that it performed better as a coating material than the constituent oxides. Finally, it was demonstrated that the nature of the core material and the sol–gel precursors for the coatings played a definite role in the electrochemical behavior of the coated cathode materials.

Acknowledgements

References

[1] K. Mizushima, P.C. Jones, P.J. Wiseman, J.B. Goodenough, Mater. Res. Bull. 15 (1980) 783.

[2] J.B. Goodenough, K. Mizushima, T. Takeda, Jpn. J. Appl. Phys. 19 (1980) 305.

[3] H.F. Wang, Y.I. Jang, B.Y. Huang, D.R. Sadoway, Y.M. Chiang, J. Electrochem. Soc. 146 (1999) 473.

[4] E. Plichita, S. Slane, M. Uchiyama, M. Salomon, D. Chua, W.B. Ebner, H.W. Lin, J. Electrochem. Soc. 136 (1989) 1865.

[5] G.G. Amatucci, J.M. Tarascon, L.C. Klein, Solid State Ionics 83 (1996) 167.

[6] J. Cho, Y.J. Kim, B. Park, Chem. Mater. 12 (2000) 3788.

[7] J. Cho, Y.J. Kim, B. Park, J. Electrochem. Soc. 148 (2001) 1110.

[8] J. Cho, Y.J. Kim, T.-J. Kim, B. Park, Angew. Chem. Int. Ed. 40 (2001) 3367.

[9] J. Cho, Y.J. Kim, T.J. Kim, B. Park, Chem. Mater. 13 (2001) 18.

[10] A.M. Kannan, L. Rabenberg, A. Manthiram, Electrochem. Solid-State Lett. 6 (2003) A16.

[11] Z. Wang, C. Wu, L. Liu, F. Wu, F. Wu, L. Chen, X. Huang, J. Electrochem. Soc. 149 (2002) A466.

[12] H.J. Kweon, S.J. Kim, D.G. Park, J. Power Sources 88 (2000) 255.

[13] M. Mladenov, R. Stoyanova, E. Zhecheva, S. Vassilev, Electrochem. Commun. 3 (2001) 410.

[14] J. Cho, C.-S. Kim, S.-I. Yoo, Electrochem. Solid-State Lett. 3 (2000) 362.

[15] X. Wang, L. Liu, L. Chen, X. Huang, Solid State Ionics 148 (2002) 335.

[16] G.T.K. Fey, H.Z. Yang, T.P. Kumar, S.P. Naik, A.S.T. Chiang, D.C. Lee, J.R. Lin, J. Power Sources 132 (2004) 172.

[17] G.T.K. Fey, Z.X. Weng, J.G. Chen, C.Z. Lu, T.P. Kumar, S.P. Naik, A.S.T. Chiang, Mater. Chem. Phys. (communicated).

[18] G.T.K. Fey, Z.X. Weng, J.G. Chen, C.Z. Lu, T.P. Kumar, S.P. Naik, A.S.T. Chiang, D.C. Lee, J.R. Lin, J. Appl. Electrochem. 34 (2004) 715.

[19] A. Bianco, M. Paci, R. Freer, J. Eur. Ceram. Soc. 18 (1998) 1235.

[20] G.T.K. Fey, C.Z. Lu, T.P. Kumar, Y.C. Chang, Surf. Coat. Technol., 2005, in press.

[21] G.T.K. Fey, J.D. Huang, T.P. Kumar, Y.C. Chang, J. Chin. Inst. Eng., 2005, in press.

[22] G.T.K. Fey, C.Z. Lu, T.P. Kumar, Surf. Coat. Technol., Communicated.

[23] J.N. Reimers, E. Rossen, C.D. Jones, J.R. Dahn, Solid State Ionics 61 (1993) 335.

[24] J.R. Dahn, U. von Sacken, C.A. Michal, Solid State Ionics 44 (1990) 87.

[25] M.S. Whittingham, M.B. Dines, J. Electrochem. Soc. 124 (1977) 1387.

[26] R. Marchand, L. Brohan, M. Tournoux, Mater. Res. Bull. 15 (1980) 1129.

[27] G.T.K. Fey, J.G. Chen, T.P. Kumar, J. Appl. Electrochem. 35 (2005) 177.

[28] R.L. Callender, C.J. Harlan, N.M. Shapiro, C.D. Jones, D.L. Callahan, M.R. Wiesner, D.B. MacQueen, R. Cook, A.R. Barron, Chem. Mater. 9 (1997) 2418.

[29] R.L. Callender, A.R. Barron, Adv. Mater. 12 (2000) 734.

[30] C.J. Harlan, A. Kareiva, D.B. MacQueen, R. Cook, A.R. Barron, Adv. Mater. 9 (1997) 68.